

A nutrient effect on the TEX₈₆ paleotemperature proxy

Ronnakrit Rattanasriampaipong^{1,2*}, Jessica E. Tierney², Jordan T. Abell³

¹University Corporation for Atmospheric Research, Boulder, CO 80307

²Department of Geosciences, The University of Arizona, Tucson, AZ 85721

³Department of Earth and Environmental Sciences, Lehigh University, Bethlehem, PA 18015

Key Points:

- Nutrient stress alters GDGT distributions in marine sediments, resulting in elevated TEX₈₆ values beyond those related to thermal effect
- Paleoclimate case studies from the Arabian Sea and Tasman Sea reveal that nutrient levels likely influenced the TEX₈₆ proxy in the past
- Explicitly accounting for nutrient effects in the proxy system will improve the accuracy of TEX₈₆-based temperature estimates

*Current address, Tucson, AZ

Corresponding author: Ronnakrit Rattanasriampaipong, ronnakritr@arizona.edu,
rrattan@ucar.edu

13 **Abstract**

14 The TEX₈₆ paleotemperature proxy is widely used for reconstructing ocean surface tem-
 15 peratures over the past 100 million years. However, archaeal culture experiments show
 16 that nutrient stress elevates TEX₈₆ values by increasing glycerol dialkyl glycerol tetraether
 17 (GDGT) cyclization. Here, we demonstrate that this “nutrient effect” is also recorded
 18 in sedimentary GDGTs. Using an expanded TEX₈₆ core-top database, we calculated TEX₈₆
 19 residuals by regressing TEX₈₆ against thermocline-integrated ocean surface temperatures.
 20 The residuals correlate negatively with surface nitrate concentrations ($\rho = -0.33; P < .001$),
 21 with stronger correlations ($\rho < -0.7; P < .001$) in regions with steep nitrate gradients. Com-
 22 parison of TEX₈₆ and U_{37'}-based reconstructions from the Arabian Sea and Tasman Sea
 23 suggests nutrient stress influenced GDGT distributions during glacial-interglacial cycles.
 24 Our findings underscore the need to account for nutrient effects in TEX₈₆ paleothermom-
 25 etry.

26 **Plain Language Summary**

27 Marine archaea help regulate the global nitrogen cycle, and their membrane lipids
 28 serve as a temperature proxy (TEX₈₆) both today and in the past. While temperature
 29 is the main driver of lipid changes, lab studies show that nutrient stress also increases
 30 lipid cyclization, potentially affecting TEX₈₆ accuracy. Here, we show that this “nutri-
 31 ent effect” is recorded in marine sediments and can be separated from the temperature
 32 signal. This effect may explain discrepancies between TEX₈₆-based temperature estimates
 33 and other proxies for surface ocean temperature, particularly in regions with strong nu-
 34 trient variations. Accounting for nutrient effects is essential to improve TEX₈₆ as a pa-
 35 leotemperature proxy.

36 **1 Introduction**

37 Reconstructing ocean temperatures is essential for understanding Earth’s climatic
 38 history (Tierney et al., 2020; Judd et al., 2024). The paleotemperature proxy TEX₈₆ (tetraether
 39 index of 86 carbons) is widely applied to reconstruct surface ocean temperatures through-
 40 out the Mesozoic–Cenozoic, particularly during greenhouse intervals (Judd et al., 2022).
 41 The proxy is based on the degree of cyclization of archaeal membrane lipids preserved
 42 in marine sediments. These lipids include isoprenoid glycerol dialkyl glycerol tetraethers
 43 (GDGTs) containing 0–4 cyclopentyl moieties (commonly referred as GDGT-n, where
 44 n denotes the number of internal rings), along with crenarchaeol (cren) and its isomer
 45 (cren')—two unique GDGTs with four cyclopentyl and one cyclohexyl moiety (Sinninghe Damst 
 46 et al., 2002). Warmer sea surface temperatures (SSTs) generally correspond to a higher
 47 proportion of cyclized GDGTs in surface (core-top) marine sediments, resulting in higher
 48 TEX₈₆ values, as defined by Schouten et al. (2002):

$$TEX_{86} = \frac{[GDGT - 2] + [GDGT - 3] + [Cren']}{[GDGT - 1] + [GDGT - 2] + [GDGT - 3] + [Cren']}$$

49 This relationship reflects homeoviscous adaptation, a physical mechanism where the de-
 50 gree of cyclization in archaeal membrane lipids adjusts to temperature. Experimental
 51 evidence, including (hyper)thermophilic (De Rosa et al., 1980; Uda et al., 2001) and mesophilic
 52 (Elling et al., 2015) archaeal cultures, along with seawater mesocosms containing mixed
 53 marine archaeal populations (Wuchter et al., 2004; Schouten et al., 2007), strongly sup-
 54 ports the use of TEX₈₆ as a reliable paleothermometer.

55 Although core-top TEX₈₆ correlates strongly with ocean surface temperatures, non-
 56 thermal factors such as archaeal community structure (Taylor et al., 2013; Villanueva
 57 et al., 2015; Hurley et al., 2018; Rattanasriampaipong et al., 2022a; van der Weijst et
 58 al., 2022) and biogeochemical conditions that impose energetic stress (Elling et al., 2014;
 59 Qin et al., 2015) also influence GDGT distributions. Notably, the role of nutrient avail-

ability remains underexplored, despite laboratory evidence showing that archaeal growth under conditions with limited electron donors (i.e., limited substrate availability; Elling et al., 2014; Hurley et al., 2016) or acceptors (i.e., low oxygen conditions; Qin et al., 2015) can enhance GDGT cyclization in archaeal cultures. Observations from both modern water columns (e.g., Hurley et al., 2018) and paleoclimate records (e.g., Junium et al., 2018; Polik et al., 2018) further suggest that nutrient availability may shape TEX₈₆ signals, potentially through its influence on archaeal metabolism and GDGT production.

Marine archaea are key ammonia oxidizers in today's oceans (Karner et al., 2001; Francis et al., 2005; Wuchter et al., 2006), playing a central role in ocean nitrification by converting ammonia to nitrite, which is subsequently oxidized to nitrate by nitrifying bacteria. The availability of these bioavailable nitrogen species regulates surface ocean productivity (Tyrrell, 1999; Yool et al., 2007) and influences archaeal metabolism (Ward, 2008; Martens-Habbena et al., 2009; Ward, 2011; Peng et al., 2016; Proctor et al., 2023). The most direct indicators for archaeal growth conditions would be ammonia oxidation rate, ammonium concentrations, or nitrite concentrations (cf. Wuchter et al., 2006; Beaman et al., 2008; Sintes et al., 2013; Smith et al., 2014; Qin et al., 2015), but measurements of these quantities are sparse and don't cover the global ocean (cf. Paulot et al., 2015; Tang et al., 2023). However, available data suggest a moderate correlation between ammonia oxidation rates and surface ocean nitrate concentrations ($\rho = 0.34$, $P < .001$; see **Figure S1**). Given that nitrate is the final product of the ocean nitrification and is widely measured, we use nitrate concentrations as a practical proxy for ammonia oxidation to investigate the influence of nutrient availability on sedimentary TEX₈₆.

2 Data and methods

2.1 Ocean temperatures and nitrate concentrations

We use the $0.25^\circ \times 0.25^\circ$ ocean temperature mean field (t_{mn}) from the 1991–2020 decadal average provided by the 2023 World Ocean Atlas (WOA23; Locarnini et al., 2024). The thermocline depth was determined as the depth at which the maximum rate of temperature change occurs in each spatial grid (see supplementary text for details). We then calculated *thermocline-integrated temperature (thermo-T)* by depth-integrating ocean temperatures down to the thermocline.

Nitrate concentrations were derived from the Copernicus Marine Environment Monitoring Service (CMEMS) global ocean biogeochemistry hindcast product (Perruche, 2018). Decadal averages of nitrate concentrations were calculated from the $0.25^\circ \times 0.25^\circ$ monthly mean fields spanning 1993–2022 using the *ncclimo* NetCDF Climatology Generator. Spatial coordinates of the dataset were then re-gridded to be consistent with the WOA23 temperature dataset. As with ocean temperatures, we calculated a *thermocline-integrated nitrate* value (referred to interchangeably as *surface ocean nitrate*).

2.2 Global TEX₈₆ core-top observations

We update the global core-top dataset previously used in the Bayesian temperature calibration model BAYSPAR ($n = 1095$; Tierney & Tingley, 2014, 2015b). The updated dataset includes 2104 core-top TEX₈₆ observations, incorporating (i) data published in previous compilation efforts (J.-H. Kim et al., 2008, 2010; Tierney & Tingley, 2014, 2015b), (ii) data published in regional studies since 2015 (Kaiser et al., 2015; J.-H. Kim et al., 2015; Rodrigo-Gámiz et al., 2015; Tierney et al., 2015; J.-H. Kim et al., 2016; Kusch et al., 2016; Pan et al., 2016; Richey & Tierney, 2016; Sinninghe Damsté, 2016; Jaeschke et al., 2017; Ceccopieri et al., 2018; Chen et al., 2018; Lo et al., 2018; Schukies, 2018; Y. Yang et al., 2018; Harning et al., 2019; Wei et al., 2020; Lamping et al., 2021; Sinninghe Damsté et al., 2022; Hagemann et al., 2023; Harning et al., 2023; Varma, Hopmans, van Kemenade, et al., 2024), and (iii) new data analyzed in the Organic Geochem-

109 istry Laboratory at the University of Arizona (see **Figure S2** for the distribution of the
 110 updated database). These data are sourced from multiple publications and laboratories.
 111 While protocols for GDGT determination using high performance liquid chromatogra-
 112 phy (HPLC)-mass spectrometry (MS) analysis have evolved over the year, we specify the
 113 method used whenever available. However, previous work suggests that older and newer
 114 HPLC-MS methods produce comparable results (cf. Hopmans et al., 2016, see Supple-
 115 **mentary Text S1 for details**). We removed samples that are heavily impacted by non-
 116 pelagic GDGT sources, based on thresholds of the Branched versus Isoprenoid Tetraether
 117 (BIT) index > 0.5 (terrestrial GDGT inputs; Hopmans et al., 2004; Weijers et al., 2006),
 118 Methane Index > 0.5 (GDGT inputs from methanotrophs; Zhang et al., 2011; B. Kim
 119 & Zhang, 2023), and %GDGT-0 > 60 (GDGT inputs from methanogens; Blaga et al.,
 120 2009; Sinninghe Damsté et al., 2012; Inglis et al., 2015).

121 Core-top TEX₈₆ observations were converted into a uniform 0.25°x0.25° spatial grid,
 122 consistent with the ocean data products. For grid cells with multiple TEX₈₆ observa-
 123 tions, median values were used for subsequent statistical analyses.

124 The dominant environmental influence on core-top TEX₈₆ is ocean temperature
 125 (Schouten et al., 2002; J.-H. Kim et al., 2008, 2010; Tierney & Tingley, 2014, 2015b).
 126 Indeed, our simple linear regression of the updated database suggest that thermocline-
 127 integrated T explains 76% ($r^2=0.76$) of the TEX₈₆ variance (**Figure 1a**). In order to
 128 isolate the secondary nutrient effect discussed here, we calculated TEX₈₆ residuals by
 129 subtracting predicted TEX₈₆ from observed values. Following J.-H. Kim et al. (2010)
 130 and Tierney and Tingley (2014, 2015b), core-top TEX₈₆ from high-latitude sites (>70°N)
 131 were excluded from linear regression, as TEX₈₆ values at these locations (SST<5) show
 132 no sensitivity to ocean surface temperature.

133 3 Results and Discussion

134 3.1 A nutrient effect on marine sedimentary TEX₈₆

135 Core-top TEX₈₆ residuals exhibit a weak but statistically significant negative cor-
 136 relation with the logarithm of thermocline-integrated nitrate concentrations ($\rho = -0.17$,
 137 $P < .001$; **Figure 1b**). A stronger relationship emerges when we restrict the regression
 138 to low-nutrient environments, defined as nitrate concentrations below 2.7 μmol/L ($\rho =$
 139 -0.33 , $P < .001$; **Figure 1b**). The low-nutrient threshold corresponds to the nitrate con-
 140 centration at which the rolling mean of TEX₈₆, calculated using a sliding window of 19
 141 data points, reaches its minimum. We tested different window sizes and selected the one
 142 that yielded the strongest correlation between nitrate and TEX₈₆ residuals.

143 While ammonia availability regulates the cellular metabolism of marine archaea
 144 (Ward, 2008, 2011; Peng et al., 2016; Proctor et al., 2023), our findings suggest that ni-
 145 trate is a reasonable proxy for identifying low-nutrient (low-ammonia) locations. The
 146 observed relationship between TEX₈₆ and nitrate indicates that archaeal communities
 147 grow more slowly (i.e., exhibit lower ammonia oxidation rates) in regions with low nu-
 148 trients, and produce GDGTs with more rings, leading to higher TEX₈₆. This trend aligns
 149 with laboratory experiments showing that archaea increase membrane permeability by
 150 synthesizing GDGTs with higher ring numbers under energy-limiting conditions (Elling
 151 et al., 2015; Hurley et al., 2016). The magnitude of elevated TEX₈₆ of about 0.1 proxy
 152 units agrees well with the experimental evidence (Hurley et al., 2016). Given the log-
 153 arithmetic nature of the regression used here, the effect of nitrate limitation spans a con-
 154 centration range of 0.1–2.5 μmol/L. For context, nitrate levels between 0.5 and 2 μmol/L
 155 are considered limiting for primary productivity in the surface ocean (Henley et al., 2020;
 156 Browning & Moore, 2023).

157 To further investigate this nutrient effect, we analyzed regional-scale patterns, fo-
 158 cusing on areas that have strong nutrient gradients and where core-top TEX₈₆ residu-

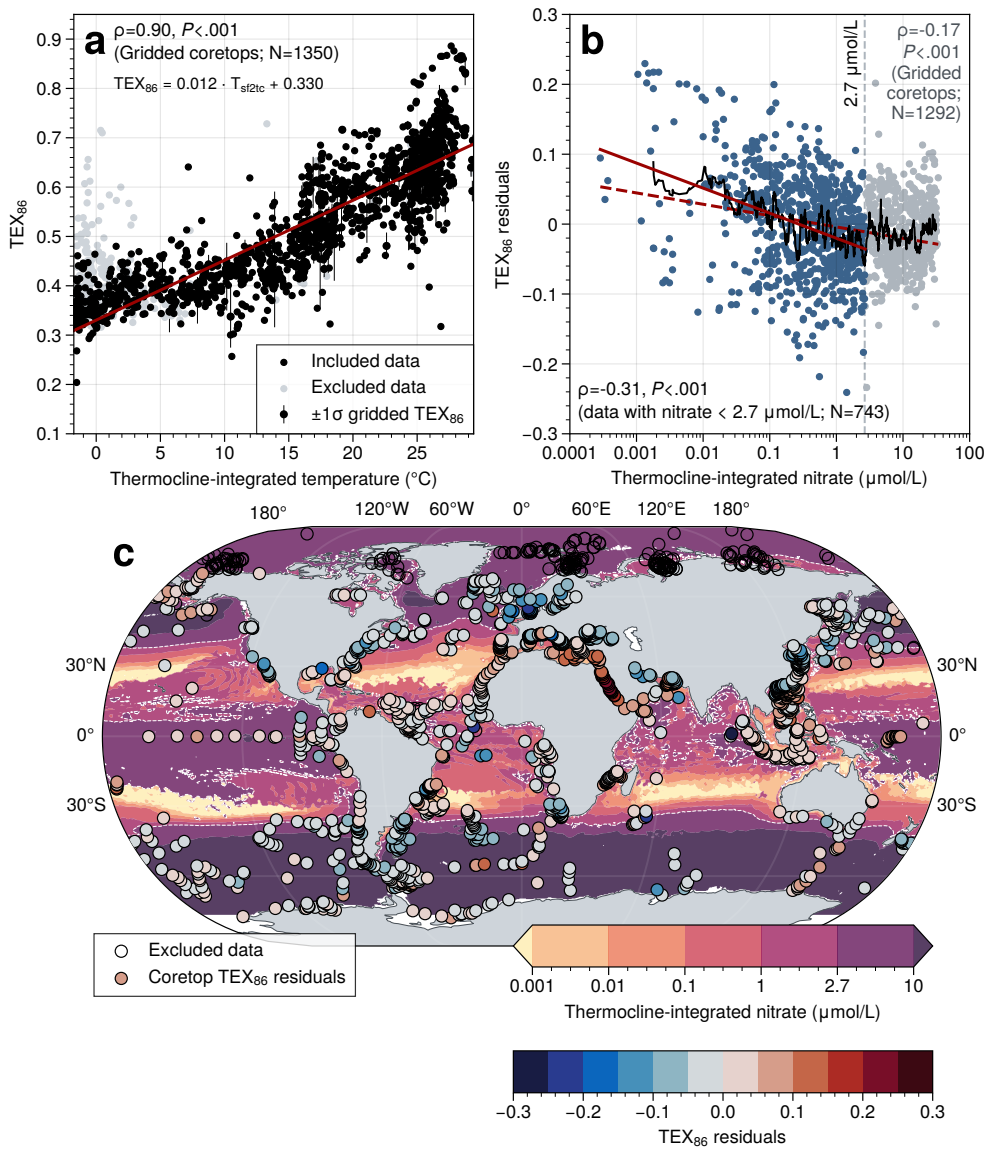


Figure 1. Elevated TEX_{86} residuals in surface marine sediments correspond to low-nutrient regions. (a) Gridded core-top TEX_{86} values exhibit a positive correlation with thermocline-integrated ocean temperature. Data north of 70°N were excluded from the regression following J.-H. Kim et al. (2010) and Tierney and Tingley (2014, 2015b). (b) Residuals of gridded core-top TEX_{86} show a weak but significant negative correlation with thermocline-integrated nitrate concentrations, suggesting a “nutrient effect.” This effect is more pronounced in low-nutrient regions (highlighted in blue), defined by a threshold of $2.7 \mu\text{mol/L}$, where the lowest rolling mean of TEX_{86} is observed. The solid black line represents the rolling mean, calculated by the sliding window of 19 data points. (c) Spatial distribution of gridded core-top TEX_{86} residuals, with higher values generally occurring in regions with low surface nitrate concentrations. Shaded contours indicate thermocline-integrated nitrate levels, with the low-nutrient threshold contour (white dashed) highlighting oligotrophic areas.

als show a strong negative correlation with nitrate. TEX₈₆ residuals from these regions show an average negative correlation with nitrate of $\rho = -0.57$ ($P < .001$; **Figure 2a**), with core-tops near the South Atlantic Subtropical Front exhibiting the strongest relationship ($\rho = -0.91$, $P < .001$; **Figure 2c**). Notably, TEX₈₆ residuals from the Red Sea show a strong nutrient effect ($\rho = -0.74$, $P < .001$; **Figure 2c**). This differs from the original study of sedimentary TEX₈₆ in the Red Sea, which did not identify a strong correlation between TEX₈₆ and nitrate (Trommer et al., 2009). This discrepancy may stem from the coarse spatial resolution ($1^\circ \times 1^\circ$) of nitrate data in the World Ocean Atlas database, which may not adequately capture fine-scale nutrient gradients in restricted basins. While earlier studies attributed anomalously high TEX₈₆ in the Red Sea to endemic clades of marine archaea (Trommer et al., 2009; J.-H. Kim et al., 2010), our findings suggest a more parsimonious alternative explanation: elevated TEX₈₆ reflects extreme nutrient stress in this oligotrophic sea.

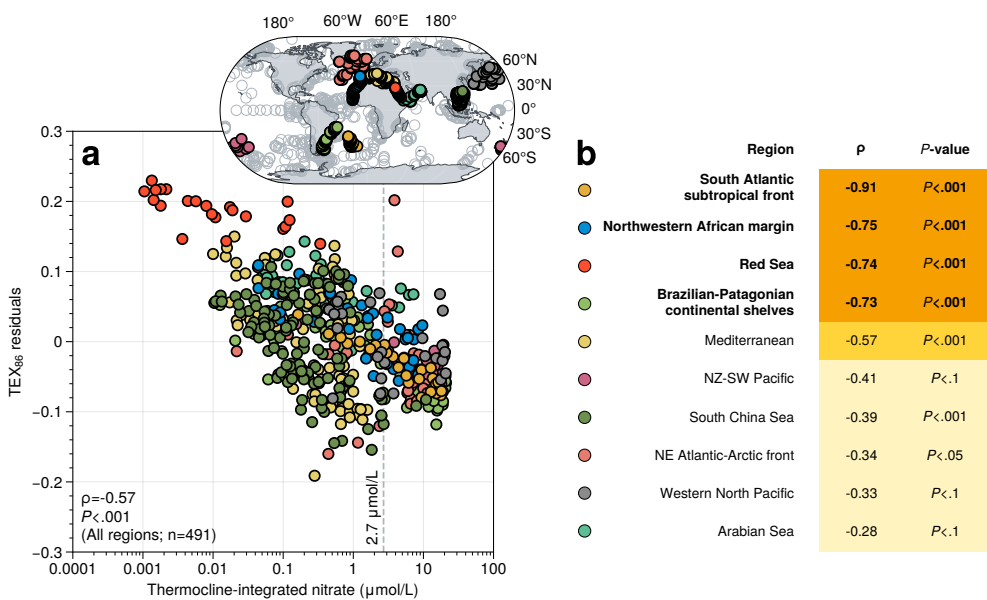


Figure 2. A pronounced nutrient effect on core-top TEX₈₆ in regions with strong nutrient gradients. (a) Scatter plot illustrating the relationship between regional gridded core-top TEX₈₆ residuals and thermocline-integrated nitrate concentrations, with an overall Spearman correlation coefficient ($\rho = -0.57$; $P < .001$; $n = 491$). The vertical dash line shows the low-nutrient threshold of $2.7 \mu\text{mol/L}$. An inset map showing core-top locations of regions with significant negative correlations between TEX₈₆ residuals and NO₃⁻ concentrations. (b) Table summarizing Spearman correlation coefficients (ρ) and associated P -values for specific regions.

3.2 Implications for TEX₈₆ paleothermometry

TEX₈₆-derived ocean temperature estimates occasionally yield anomalously high values that diverge from other proxies and paleoclimate expectations. Here, we explore two paleoclimate scenarios in which nutrient stress may account for the discrepancies between TEX₈₆-derived temperatures and SST estimates from the U_{37'} proxy—an independent organic paleotemperature proxy based on unsaturated ketones produced by coccolithophores. Although multiple calibrations for TEX₈₆ exist, some of which are non-linear (J.-H. Kim et al., 2010), in these examples we convert TEX₈₆ to temperatures using the simple linear regression with thermocline-integrated T developed above to high-

light deviations from the general linear thermal effect. For the $U_{37}^{K'}$ data, we use the Bayesian calibration BAYSPLINE (Tierney & Tingley, 2018), which is linear up to temperatures of 25°C, at which point the proxy has a non-linear response as it approaches the maximum possible value of 1.

3.2.1 Denitrification dynamics in the Arabian Sea upwelling zone

Reconstructed ocean temperatures from $U_{37}^{K'}$ and TEX₈₆ records in the Arabian Sea capture the overall warming trend since the last deglaciation, marking the transition from the Last Glacial Maximum to the Holocene interglacial (Figure 3; Huguet et al., 2006; Tierney et al., 2016). However, a persistent feature is that TEX₈₆-derived temperatures remain consistently warmer than $U_{37}^{K'}$ -based SSTs throughout most of the past 20,000 years (Figure 3b). This discrepancy contrasts with modern observations, which indicate that thermocline temperatures at these sites are slightly cooler than SSTs.

A particularly striking feature is the anomalous TEX₈₆ warming during the Younger Dryas (YD, ca. 12.9–11.7 thousand years ago, ka; Rasmussen et al., 2006) and Heinrich Stadial 1 (HS1, ca. 17.5–14.5 ka; McManus et al., 2004; Broecker & Barker, 2007) events. During these intervals, TEX₈₆-derived temperatures increase sharply, whereas $U_{37}^{K'}$ -based SSTs do not record warming (Figure 3b; Huguet et al., 2006; Tierney et al., 2016). In fact, both the $U_{37}^{K'}$ records and the TraCE-21ka paleoclimate model simulation—a fully coupled simulation of Transient Climate Evolution over the past 21,000 years—indicate surface cooling during the YD and HS1, reflecting broader Northern Hemisphere climate dynamics (Sonzogni et al., 1998; Schulte & Müller, 2001; Huguet et al., 2006; Tierney et al., 2016). While Tierney et al. (2016) attributed this discrepancy to TEX₈₆ recording subsurface water warming, the magnitude of the TEX₈₆ warming anomalies—up to 7°C from the pre-event baseline (Figure 3b–c)—is unrealistically large. Altogether, these observations suggest that TEX₈₆ is influenced by additional environmental factors beyond temperature alone.

Core sites NIOP-C2_905_PC and SO42-74KL are located at the periphery of present-day low-nutrient zones (Figure 3d), making them particularly sensitive to nutrient dynamics. We propose that nutrient stress on archaeal communities in the Arabian Sea has been persistent since the last deglaciation, as indicated by present-day nitrate concentrations. Under today's interglacial conditions, a high nutrient “blob” is present in this region, but it may have dissipated during past cooling episodes. Weakened monsoon winds during these periods (Tierney et al., 2016) likely reduced upwelling, limiting the supply of nutrient-rich waters to the surface. This could have induced nutrient stress in marine archaea, leading to the production of more cyclic GDGTs and higher TEX₈₆ values.

This interpretation is supported by denitrification proxy records from the Arabian Sea. Lower bulk sediment $\delta^{15}\text{N}$ values during the YD and HS1 indicate reduced denitrification, consistent with weakened upwelling and lower nitrate availability in surface waters (Figure 3c; Altabet et al., 1995; Suthhof et al., 2001; Altabet et al., 2002; Ivanochko et al., 2005). Moreover, after interpolating all time series ($U_{37}^{K'}$, TEX₈₆, and $\delta^{15}\text{N}$) onto a common time step, we find that TEX₈₆ T anomalies (Thermo-T_{TEX₈₆} - SST _{$U_{37}^{K'}$}) exhibit a strong negative correlation with bulk sediment $\delta^{15}\text{N}$ during YD and HS1 (see Figure SI3a–b). By subtracting the Holocene mean values from the TEX₈₆ records, we de-trend the data and find that temperature anomalies of up to 7°C correspond to increases of up to 0.1 proxy units in TEX₈₆ (see Figure SI3c–d), which mirrors the trends observed in modern core-top records.

Collectively, these lines of evidence suggest that TEX₈₆ temperatures in the Arabian Sea are sensitive to nutrient availability in surface waters. Reduced upwelling during the YD and HS1 events likely amplify the nutrient stress on marine archaea, resulting in anomalously high TEX₈₆ values. It is important to note that we do not observe a comparable TEX₈₆ warming anomaly at the end of the Last Glacial Maximum (LGM,

ca. 20–19 ka; Clark et al., 2009). This suggests that surface ocean circulation patterns, monsoonal dynamics, and nutrient availability differed between the nearly steady-state conditions of the LGM and the transient cooling events of the deglacial period. Future work should investigate longer records spanning the full LGM to determine whether nutrient stress systematically influenced TEX₈₆ signals under different climate regimes.

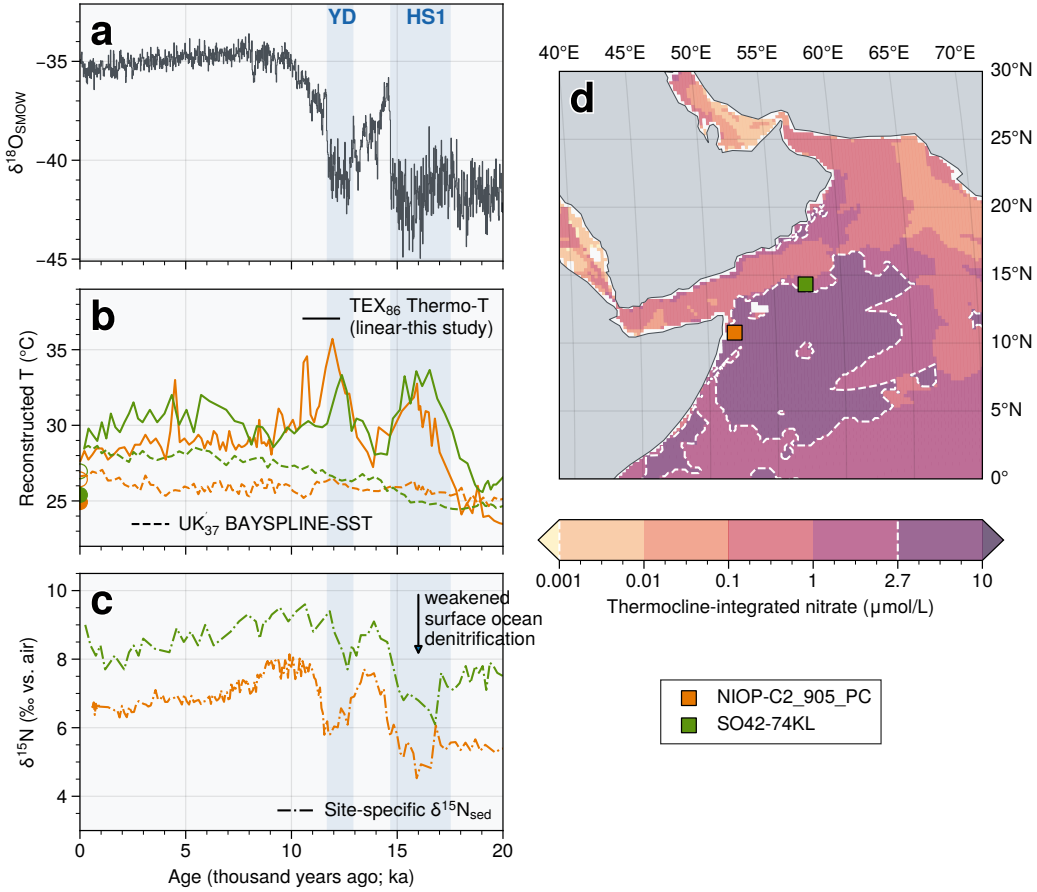


Figure 3. Anomalously warm TEX₈₆ signals during the Younger Dryas (YD) and Heinrich Stadial 1 (HS1) in the Arabian Sea. (a) Northern Greenland Ice Project (NGRIP) ice core $\delta^{18}\text{O}$ record (Seierstad et al., 2014), a proxy for Northern Hemisphere temperature changes, highlighting cooling during YD (ca. 12.9–11.7 kyr BP; Rasmussen et al., 2006) and HS1 (ca. 17.5–14.5 kyr BP; McManus et al., 2004; Broecker & Barker, 2007). (b) Reconstructed ocean temperatures from sediment cores NIOP-C2_905_PC and SO42-74KL in the Arabian Sea. $\text{U}_{37}^{K'}$ -derived sea surface temperature (SST) records are based on the BAYSPLINE calibration (Tierney & Tingley, 2018), while TEX₈₆-derived thermocline-integrated temperatures (thermo-T) are based on the linear regression of the updated core-top dataset (Figure 1a). Original proxy data were retrieved from Huguet et al. (2006). Modern SST (open circles) and thermo-T (filled circles) are indicated. (c) Bulk sediment $\delta^{15}\text{N}$ records from NIOP-C2_905_PC (Ivanochko et al., 2005) and SO42-74KL (Suthhof et al., 2001), serving as a proxy for surface ocean denitrification. The records indicate reduced denitrification during cooling events. Data sourced from the global ocean nitrogen isotope database (Tesdal et al., 2013). (d) Map showing core locations. Shaded contours represent modern surface nitrate concentrations, with the white dashed contour marking the low-nutrient area ($<2.7 \mu\text{mol/L}$ surface nitrate) of the Arabian Sea.

237 **3.2.2 South Pacific Subtropical Gyre poleward expansion**

238 Our second example investigates ocean temperature changes in the Tasman Sea,
 239 a location associated with a strong north-south gradient in nutrients in the present-day
 240 (see **Figure 4e**). $U_{37}^{K'}$ and TEX_{86} temperatures largely track each other over the past
 241 150,000 years and recapitulate the climate history since the penultimate deglaciation (**Figure**
 242 **4**). However, TEX_{86} -derived Ts occasionally exceed 25°C, which is implausibly high for
 243 these core locations—suggesting that another factor beyond temperature is influencing
 244 the proxy.

245 Today, DSDP Site 591 is located within the Tasman Front, which is a component
 246 of the low-nutrient western boundary of the South Pacific Subtropical Gyre (SPSTG).
 247 IODP Site U1510, while still within the gyre's low-nutrient zone, is positioned approx-
 248 imately 5 degrees farther south, where surface waters are more quiescent and impacted
 249 primarily by eddies shed from the East Australian Current (4d) ([Talley et al., 2011](#); [Ganachaud et al., 2014](#); [Sloyan & O'Kane, 2015](#)). Core-top TEX_{86} residuals from the adjacent south-
 250 west Pacific (see the NZ-SW Pacific region in **Figure 2**) also exhibit a pronounced nu-
 251 trient effect. Visual inspection of the TEX_{86} records reveals episodic warming events in
 252 which TEX_{86} -derived thermo-Ts temporarily exceed SSTs inferred from $U_{37}^{K'}$. These events
 253 generally occur near the onset of interglacial periods (i.e., odd-numbered marine isotope
 254 stages; see **Figures 4a–c**).

255 Conversely, during glacial periods TEX_{86} -derived thermo-Ts are typically lower than
 256 $U_{37}^{K'}$ -derived SSTs, consistent with the distinct depth habitats recorded by the proxies—
 257 TEX_{86} reflecting subsurface thermocline conditions dominated by archaeal populations
 258 and $U_{37}^{K'}$ capturing surface conditions via haptophyte algae. Nevertheless, even within
 259 glacial intervals, transient TEX_{86} warming signals are observed at both sites, with the
 260 effects being stronger and more frequent at DSDP Site 591. This pattern is likely due
 261 to DSDP Site 591's location, as it lies closer to the western edge of the gyre center. With
 262 these more nutrient depleted waters, the site experiences more intense nutrient limita-
 263 tion, amplifying the nutrient-driven bias in the TEX_{86} proxy.

264 We propose that the warming bias in TEX_{86} temperatures during warm intervals
 265 reflect changes in surface nutrient availability driven by enhanced upper-ocean strati-
 266 fication, the poleward expansion of the SPSTG, or a combination of both mechanisms.
 267 Modern observations indicate that increasing surface temperatures and weaker winds pro-
 268 mote stratification in the Tasman Sea's upper layers, with satellite ocean color and al-
 269 timetry data (*cf.* [Tilburg et al., 2002](#)) showing a clear intensification of this stratifica-
 270 tion on seasonal timescales. Although seasonal variations occur on shorter timescales,
 271 they provide a proxy for the behavior of the system under sustained warm climate con-
 272 ditions.

273 Furthermore, paleoclimate reconstructions from previous studies suggest that the
 274 mean positions of the Tasman Front ([Martínez, 1994](#); [Kawagata, 2001](#)) and the Subtrop-
 275 ical Front in the southwest Pacific ([Sikes et al., 2009](#); [Hayward et al., 2012](#); [Bostock et al., 2015](#)) migrate poleward during interglacial periods. Pacific model simulations also
 276 indicate that warming leads to the expansion of subtropical gyres ([Polovina et al., 2011](#);
 277 [H. Yang et al., 2020](#)), a process that can intensify oligotrophic conditions at these sites.
 278 In our view, whether stratification increases primarily due to thermal effects, front mi-
 279 gration, or gyre expansion, the outcome is a reduction in nutrient availability at the sur-
 280 face. This nutrient limitation could trigger physiological shifts in marine archaea—altering
 281 GDGT production and distribution—and ultimately lead to an overestimation of TEX_{86} -
 282 based temperatures during interglacial intervals.

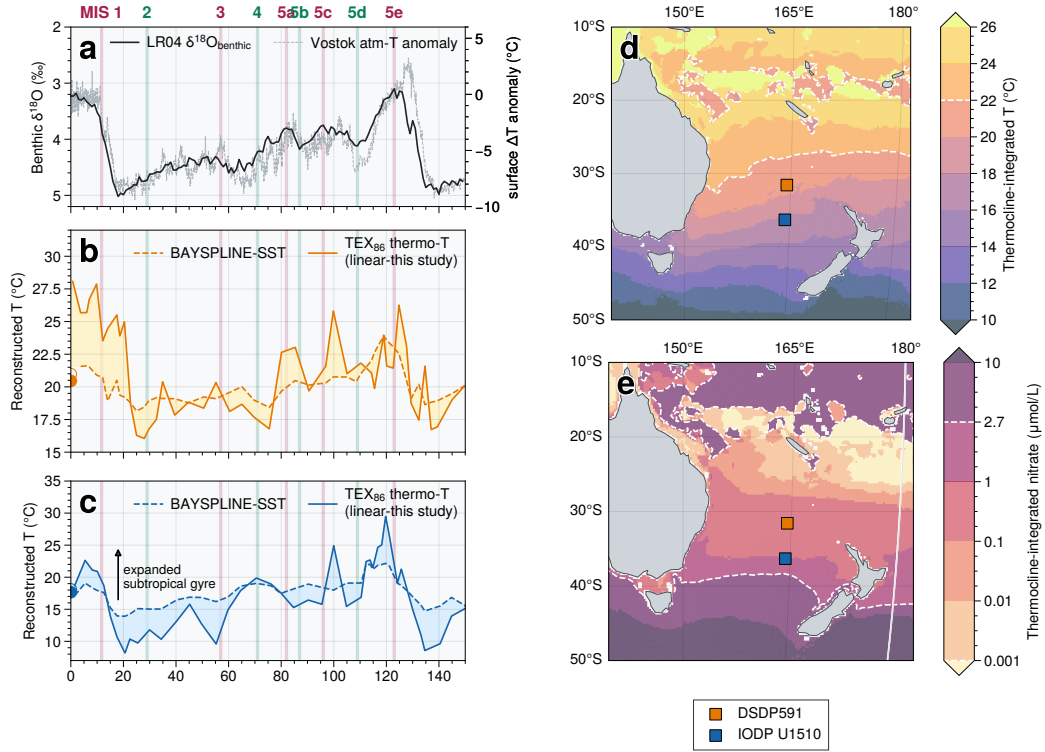


Figure 4. Nutrient effect on TEX₈₆ records in the Tasman Sea. (a) LR04 global benthic $\delta^{18}\text{O}$ stack (Lisiecki & Raymo, 2005) and Vostok atmospheric temperature anomalies (Petit et al., 1999), representing climate variability across glacial-interglacial cycles since the penultimate deglaciation (ca. 138 ka; Govin et al., 2015). (b, c) Time series of reconstructed ocean temperatures from ocean drilling sites DSDP 591 and IODP U1510 in the Tasman Sea. UK₃₇-derived sea surface temperatures (SST; dashed) are based on the BAYSPLINE calibration (Tierney & Tingley, 2018), while TEX₈₆-derived thermocline-integrated temperatures (thermo-T; solid) are based on the linear regression from this study. Modern SST (open circles) and thermo-T (filled circles) at each site are indicated. Vertical lines indicate the onset of Marine Isotope Stages (MIS) 1 to 5e, color-coded as glacial (teal) and interglacial (pink) periods (Lisiecki & Raymo, 2005). (d, e) Maps showing core locations in the Tasman Sea. Shaded contours represent modern (d) thermocline-integrated temperatures and (e) nitrate concentrations. The white dashed contour marks the 22°C isotherm and the low-nutrient core (<2.7 $\mu\text{mol/L}$ surface nitrate) of the South Pacific Subtropical Gyre, respectively.

285 **4 Conclusions**

286 Our study demonstrates that the “nutrient effect” is recorded in sedimentary TEX₈₆,
 287 wherein low-nutrient regions of the global ocean are associated with higher TEX₈₆ val-
 288 ues. This observation is consistent with laboratory studies showing that nutrient lim-
 289 itation leads to higher GDGT cyclization (Elling et al., 2014; Hurley et al., 2016), and
 290 the magnitude of increased cyclization observed in modern environments aligns well with
 291 experimental evidence (Hurley et al., 2016). Furthermore, comparisons between TEX₈₆
 292 and U_{37'} paleotemperature reconstructions in the Arabian Sea and Tasman Sea indicate
 293 that nutrient stress has significantly influenced GDGT distributions, albeit with region-
 294 specific signatures—manifesting as cooling events in the Arabian Sea versus anomalously
 295 high TEX₈₆ temperatures during warm intervals in the Tasman Sea.

296 These findings suggest that previous TEX₈₆-based temperature reconstructions—especially
 297 for warm intervals—may require reevaluation. Integrating TEX₈₆ with independent prox-
 298 ies such as $\delta^{15}\text{N}$ and paleoproductivity markers could help resolve discrepancies among
 299 proxies and between proxy data and climate model simulations—e.g., during the early
 300 Eocene (e.g., Douglas et al., 2014), the PETM (e.g., Kozdon & Kelly, 2024), and OAEs.
 301 Nutrient stress may also explain extreme TEX₈₆ values in deep-time events such as the
 302 PETM (cf. Zachos et al., 2001, 2008) and OAEs (cf. Kuypers et al., 2001; van Helmond
 303 et al., 2014). During these intervals, increased weathering likely supplied nutrients to coastal
 304 oceans, but intensified warming and stronger upper-ocean stratification restricted ver-
 305 tical nutrient supply in the open ocean (Erbacher et al., 2001). This could have led to
 306 lower nitrate concentrations, enhanced nutrient stress on marine archaea, and overpro-
 307 duction of cyclic GDGTs, resulting in anomalously high TEX₈₆ values (>0.8) (e.g., Forster,
 308 Schouten, Baas, & Sinninghe Damsté, 2007; Forster, Schouten, Moriya, et al., 2007; Sin-
 309 ninghe Damsté et al., 2010). Our findings highlight the importance of considering nu-
 310 trient stress when interpreting TEX₈₆ signals in both recent and deep-time climate re-
 311 constructions.

312 Recognizing the dual influence of temperature and nutrient availability on GDGT
 313 production is crucial for improving TEX₈₆-based paleotemperature reconstructions and
 314 climate models. Future studies should quantify nutrient effects on GDGT cyclization across
 315 diverse archaeal clades, while high-resolution oceanographic observations in regions with
 316 strong nutrient gradients will improve proxy calibrations. Controlled culture experiments—
 317 similar to those reported by Hurley et al. (2016)—should explore a broader range of nu-
 318 trient conditions to refine our mechanistic understanding of GDGT production. Addi-
 319 tionally, the limitations of low-resolution oceanographic datasets in capturing fine-scale
 320 nutrient gradients, particularly in semi-enclosed seas, highlight the need for regional syn-
 321 theses that integrate TEX₈₆ with nutrient and archaeal community composition data.
 322 As warming continues to alter ocean stratification and nutrient distributions, explicitly
 323 incorporating nutrient effects into TEX₈₆ calibrations will enhance the accuracy of past
 324 climate reconstructions and future projections, improving its reliability as a paleotem-
 325 perature proxy.

326 **Open Research Section**

327 In this study, we update the core-top TEX₈₆ dataset by integrating previous cal-
 328 ibration compilations (J.-H. Kim et al., 2008, 2010; Tierney & Tingley, 2014, 2015b; Rat-
 329 tanasriampaipong et al., 2022a; Hagemann et al., 2023; Varma, Hopmans, van Kem-
 330enda, et al., 2024). These datasets are available via NOAA-NCEI (Tierney & Tingley,
 331 2015a), Figshare (Rattanasriampaipong et al., 2022b), and PANGAEA (Hagemann et
 332 al., 2023; Varma, Hopmans, van Kemenda, et al., 2024). A full list of original data sources
 333 is provided in Table S1.

All geochemical proxy datasets, ocean data products, and analysis codes needed to reproduce our results are publicly accessible on Zenodo ([Rattanasriampaipong et al., 2025](#)) and GitHub (<https://github.com/PaleoLipidRR/nutrient-effect-on-TEX>). The analyses were performed using Python 3.10 ([Python 3.10, 2010](#)) with key libraries including NumPy ([Harris et al., 2020](#)), Pandas ([McKinney, 2010](#)), and Xarray ([Hoyer & Hamman, 2017](#)). Statistical work utilized SciPy ([Virtanen et al., 2020](#)) and scikit-learn ([Pedregosa et al., 2011](#)), while figures were generated using Matplotlib ([Hunter, 2007](#)) and enhanced with the Proplot wrapper (<https://proplot.readthedocs.io/en/stable/>). A complete list of dependencies is provided in an exported .yml file in the GitHub repository.

We also used data from the EU Copernicus Marine Service Information's Global Ocean Biogeochemistry Hindcast product (<https://doi.org/10.48670/moi-00019>), ocean temperature data from the 2023 World Ocean Atlas ([Locarnini et al., 2024](#)), and datasets from the global nitrification ([Tang et al., 2023](#)) and ocean nitrogen isotope databases ([Tesdal et al., 2013](#)).

Acknowledgments

This work was supported by the NOAA Climate and Global Change Postdoctoral Fellowship Program, administered by UCAR's Cooperative Programs for the Advancement of Earth System Science (CPAESS) under the NOAA Science Collaboration Program award (Grant number #NA21OAR4310383).

References

- Altabet, M. A., Francois, R., Murray, D. W., & Prell, W. L. (1995). Climate-related variations in denitrification in the Arabian Sea from sediment $^{15}\text{N}/^{14}\text{N}$ ratios. *Nature*, 373(6514), 506–509. doi: 10.1038/373506a0
- Altabet, M. A., Higginson, M. J., & Murray, D. W. (2002). The effect of millennial-scale changes in Arabian Sea denitrification on atmospheric CO₂. *Nature*, 415(6868), 159–162. doi: 10.1038/415159a
- Beman, J. M., Popp, B. N., & Francis, C. A. (2008). Molecular and biogeochemical evidence for ammonia oxidation by marine Crenarchaeota in the Gulf of California. *The ISME Journal*, 2(4), 429–441. Retrieved from <https://doi.org/10.1038/ismej.2007.118> doi: 10.1038/ismej.2007.118
- Blaga, C. I., Reichart, G.-J., Heiri, O., & Sinninghe Damsté, J. S. (2009). Tetraether membrane lipid distributions in water-column particulate matter and sediments: a study of 47 European lakes along a north–south transect. *Journal of Paleolimnology*, 41(3), 523–540.
- Bostock, H. C., Hayward, B. W., Neil, H. L., Sabaa, A. T., & Scott, G. H. (2015). Changes in the position of the Subtropical Front south of New Zealand since the last glacial period. *Paleoceanography*, 30(7), 824–844. Retrieved from <https://doi.org/10.1002/2014PA002652> doi: <https://doi.org/10.1002/2014PA002652>
- Broecker, W., & Barker, S. (2007). A 190‰ drop in atmosphere's $\Delta^{14}\text{C}$ during the "Mystery Interval" (17.5 to 14.5 kyr). *Earth and Planetary Science Letters*, 256(1), 90–99. doi: <https://doi.org/10.1016/j.epsl.2007.01.015>
- Browning, T. J., & Moore, C. M. (2023). Global analysis of ocean phytoplankton nutrient limitation reveals high prevalence of co-limitation. *Nature Communications*, 14(1), 5014. Retrieved from <https://doi.org/10.1038/s41467-023-40774-0> doi: 10.1038/s41467-023-40774-0
- Ceccopieri, M., Carreira, R. S., Wagener, A. L. R., Hefter, J. H., & Mollenhauer, G. (2018). On the application of alkenone- and GDGT-based temperature proxies in the south-eastern Brazilian continental margin. *Organic Geochemistry*, 126, 43–56. doi: 10.1016/j.orggeochem.2018.10.009

- 385 Chen, J., Hu, P., Li, X., Yang, Y., Song, J., Li, X., ... Lü, X. (2018). Impact of
 386 water depth on the distribution of iGDGTs in the surface sediments from the
 387 northern South China Sea: applicability of TEX86 in marginal seas. *Frontiers*
 388 of Earth Science, 12(1), 95–107. doi: 10.1007/s11707-016-0620-1
- 389 Clark, P. U., Dyke, A. S., Shakun, J. D., Carlson, A. E., Clark, J., Wohlfarth, B.,
 390 ... McCabe, A. M. (2009). The Last Glacial Maximum. *Science*, 325(5941),
 391 710–714. Retrieved from <https://doi.org/10.1126/science.1172873> doi:
 392 10.1126/science.1172873
- 393 De Rosa, M., Esposito, E., Gambacorta, A., Nicolaus, B., & Bu'Lock, J. D. (1980).
 394 Effects of temperature on ether lipid composition of *Caldariella aci-*
 395 *dophila*. *Phytochemistry*, 19(5), 827–831. doi: 10.1016/0031-9422(80)
 396 85120-X
- 397 Douglas, P. M. J., Affek, H. P., Ivany, L. C., Houben, A. J. P., Sijp, W. P., Sluijs,
 398 A., ... Pagani, M. (2014). Pronounced zonal heterogeneity in Eocene southern
 399 high-latitude sea surface temperatures. *Proceedings of the National Academy of*
 400 *Sciences of the U.S.A.*, 111(18), 6582–6587. doi: 10.1073/pnas.1321441111
- 401 Elling, F. J., Könneke, M., Lipp, J. S., Becker, K. W., Gagen, E. J., & Hinrichs, K.-
 402 U. (2014). Effects of growth phase on the membrane lipid composition of the
 403 thaumarchaeon *Nitrosopumilus maritimus* and their implications for archaeal
 404 lipid distributions in the marine environment. *Geochimica et Cosmochimica*
 405 *Acta*, 141, 579–597. doi: 10.1016/j.gca.2014.07.005
- 406 Elling, F. J., Könneke, M., Mußmann, M., Greve, A., & Hinrichs, K.-U. (2015).
 407 Influence of temperature, pH, and salinity on membrane lipid composition
 408 and TEX86 of marine planktonic thaumarchaeal isolates. *Geochimica et Cos-*
 409 *mochimica Acta*, 171, 238–255. doi: 10.1016/j.gca.2015.09.004
- 410 Erbacher, J., Huber, B. T., Norris, R. D., & Markey, M. (2001). Increased
 411 thermohaline stratification as a possible cause for an ocean anoxic event
 412 in the Cretaceous period. *Nature*, 409(6818), 325–327. Retrieved from
 413 <https://doi.org/10.1038/35053041> doi: 10.1038/35053041
- 414 Forster, A., Schouten, S., Baas, M., & Sinninghe Damsté, J. S. (2007). Mid-
 415 Cretaceous (Albian–Santonian) sea surface temperature record of the
 416 tropical Atlantic Ocean. *Geology*, 35(10), 919–922. Retrieved from
 417 <https://doi.org/10.1130/G23874A.1> doi: DOI:10.1130/G23874A.1
- 418 Forster, A., Schouten, S., Moriya, K., Wilson, P. A., & Sinninghe Damsté, J. S.
 419 (2007). Tropical warming and intermittent cooling during the Cenoma-
 420 nian/Turonian oceanic anoxic event 2: Sea surface temperature records
 421 from the equatorial Atlantic. *Paleoceanography*, 22(1). Retrieved from
 422 <https://doi.org/10.1029/2006PA001349> doi: <https://doi.org/10.1029/2006PA001349>
- 423 Francis, C. A., Roberts, K. J., Beman, J. M., Santoro, A. E., & Oakley, B. B.
 424 (2005). Ubiquity and diversity of ammonia-oxidizing archaea in water columns
 425 and sediments of the ocean. *Proceedings of the National Academy of Sciences*
 426 of the U.S.A., 102(41), 14683–14688. doi: 10.1073/pnas.0506625102
- 427 Ganachaud, A., Cravatte, S., Melet, A., Schiller, A., Holbrook, N. J., Sloyan, B. M.,
 428 ... Send, U. (2014). The Southwest Pacific Ocean circulation and climate
 429 experiment (SPICE). *Journal of Geophysical Research: Oceans*, 119(11),
 430 7660–7686. Retrieved from <https://doi.org/10.1002/2013JC009678> doi:
 431 <https://doi.org/10.1002/2013JC009678>
- 432 Govin, A., Capron, E., Tzedakis, P. C., Verheyden, S., Ghaleb, B., Hillaire-Marcel,
 433 C., ... Zahn, R. (2015). Sequence of events from the onset to the demise
 434 of the Last Interglacial: Evaluating strengths and limitations of chronolo-
 435 gies used in climatic archives. *Quaternary Science Reviews*, 129, 1–36. doi:
 436 <https://doi.org/10.1016/j.quascirev.2015.09.018>
- 437 Hagemann, J. R., Lembke-Jene, L., Lamy, F., Vorrath, M.-E., Kaiser, J., Müller, J.,
 438 ... Tiedemann, R. (2023). Collection of GDGT-derived temperatures of 22
 439

- 440 new sites at the Chilean margin, supplemented by various previously published
 441 sites. [Dataset]. PANGAEA. doi: 10.1594/PANGAEA.964270
- 442 Harning, D. J., Andrews, J. T., Belt, S. T., Cabedo-Sanz, P., Geirsdottir, A., Dildar,
 443 N., ... Sepúlveda, J. (2019). Sea Ice Control on Winter Subsurface Tempera-
 444 tures of the North Iceland Shelf During the Little Ice Age: A TEX86 Calibra-
 445 tion Case Study. *Paleoceanography and Paleoceanography*, 34(6), 1006–1021.
 446 doi: 10.1029/2018PA003523
- 447 Harning, D. J., Holman, B., Woelders, L., Jennings, A. E., & Sepúlveda, J. (2023).
 448 Biomarker characterization of the North Water Polynya, Baffin Bay: implica-
 449 tions for local sea ice and temperature proxies. *Biogeosciences*, 20(1), 229–
 450 249. Retrieved from <https://doi.org/10.1594/PANGAEA.956212>
 451 https://bg.copernicus.org/articles/20/229/2023/ doi: 10.5194/bg-20-229-2023
- 452 Harris, C. R., Millman, K. J., van der Walt, S. J., Gommers, R., Virtanen, P., Cour-
 453 napeau, D., ... others (2020). Array programming with NumPy. *Nature*,
 454 585(7825), 357–362.
- 455 Hayward, B. W., Sabaa, A. T., Kolodziej, A., Crundwell, M. P., Steph, S., Scott,
 456 G. H., ... Grenfell, H. R. (2012). Planktic foraminifera-based sea-surface
 457 temperature record in the Tasman Sea and history of the Subtropical Front
 458 around New Zealand, over the last one million years. *Marine Micropaleon-*
 459 *tology*, 82-83, 13–27. Retrieved from <https://www.sciencedirect.com/science/article/pii/S0377839811001150> doi: <https://doi.org/10.1016/j.marmicro.2011.10.003>
- 460 Henley, S. F., Porter, M., Hobbs, L., Braun, J., Guillaume-Castel, R., Venables,
 461 E. J., ... Cottier, F. (2020). Nitrate supply and uptake in the Atlantic
 462 Arctic sea ice zone: seasonal cycle, mechanisms and drivers. *Philosophical
 463 Transactions of the Royal Society A: Mathematical, Physical and Engineering
 464 Sciences*, 378(2181), 20190361. Retrieved from <https://doi.org/10.1098/rsta.2019.0361> doi: 10.1098/rsta.2019.0361
- 465 Hopmans, E. C., Schouten, S., & Sinninghe Damsté, J. S. (2016). The effect of
 466 improved chromatography on GDGT-based palaeoproxies. *Organic Geochem-*
 467 *istry*, 93, 1–6. Retrieved from <https://www.sciencedirect.com/science/article/pii/S0146638015002387> doi: <https://doi.org/10.1016/j.orggeochem.2015.12.006>
- 468 Hopmans, E. C., Weijers, J. W. H., Schefuß, E., Herfort, L., Sinninghe Damsté,
 469 J. S., & Schouten, S. (2004). A novel proxy for terrestrial organic matter
 470 in sediments based on branched and isoprenoid tetraether lipids. *Earth and
 471 Planetary Science Letters*, 224(1), 107–116. doi: 10.1016/j.epsl.2004.05.012
- 472 Hoyer, S., & Hamman, J. (2017). xarray: N-d labeled arrays and datasets in Python.
 473 *Journal of Open Research Software*, 5(1), 10.
- 474 Huguet, C., Kim, J.-H., Sinninghe Damsté, J. S., & Schouten, S. (2006). Recon-
 475 struction of sea surface temperature variations in the Arabian Sea over the last
 476 23 kyr using organic proxies (TEX86 and U37K'). *Paleoceanography*, 21(3).
 477 doi: 10.1029/2005pa001215
- 478 Hunter, J. D. (2007). Matplotlib: A 2d graphics environment. *Computing in Science
 479 & Engineering*, 9(3), 90–95.
- 480 Hurley, S. J., Elling, F. J., Könneke, M., Buchwald, C., Wankel, S. D., Santoro,
 481 A. E., ... Pearson, A. (2016). Influence of ammonia oxidation rate on thaum-
 482 marchaeal lipid composition and the TEX86 temperature proxy. *Proceedings
 483 of the National Academy of Sciences of the U.S.A.*, 113(28), 7762–7767. doi:
 484 10.1073/pnas.1518534113
- 485 Hurley, S. J., Lipp, J. S., Close, H. G., Hinrichs, K.-U., & Pearson, A. (2018). Dis-
 486 tribution and export of isoprenoid tetraether lipids in suspended particulate
 487 matter from the water column of the Western Atlantic Ocean. *Organic Geo-
 488 chemistry*, 116, 90–102. doi: 10.1016/j.orggeochem.2017.11.010
- 489 Inglis, G. N., Farnsworth, A., Lunt, D., Foster, G. L., Hollis, C. J., Pagani, M., ...

- Pancost, R. D. (2015). Descent toward the Icehouse: Eocene sea surface cooling inferred from GDGT distributions. *Paleoceanography*, 30(7), 1000–1020. doi: 10.1002/2014pa002723
- Ivanochko, T. S., Ganeshram, R. S., Brummer, G.-J. A., Ganssen, G., Jung, S. J. A., Moreton, S. G., & Kroon, D. (2005). Variations in tropical convection as an amplifier of global climate change at the millennial scale. *Earth and Planetary Science Letters*, 235(1), 302–314. doi: 10.1016/j.epsl.2005.04.002
- Jaeschke, A., Wengler, M., Hefter, J., Ronge, T. A., Geibert, W., Mollenhauer, G., ... Lamy, F. (2017). A biomarker perspective on dust, productivity, and sea surface temperature in the Pacific sector of the Southern Ocean. *Geochimica et Cosmochimica Acta*, 204, 120–139. doi: 10.1016/j.gca.2017.01.045
- Judd, E. J., Tierney, J. E., Huber, B. T., Wing, S. L., Lunt, D. J., Ford, H. L., ... Zhang, Y. G. (2022). The PhanSST global database of Phanerozoic sea surface temperature proxy data. *Scientific Data*, 9(1). doi: 10.1038/s41597-022-01826-0
- Judd, E. J., Tierney, J. E., Lunt, D. J., Montañez, I. P., Huber, B. T., Wing, S. L., & Valdes, P. J. (2024). A 485-million-year history of Earth's surface temperature. *Science*, 385(6715), eadk3705. doi: 10.1126/science.adk3705
- Junium, C. K., Meyers, S. R., & Arthur, M. A. (2018). Nitrogen cycle dynamics in the Late Cretaceous Greenhouse. *Earth and Planetary Science Letters*, 481, 404–411. doi: 10.1016/j.epsl.2017.10.006
- Kaiser, J., Schouten, S., Kilian, R., Arz, H. W., Lamy, F., & Sinninghe Damsté, J. S. (2015). Isoprenoid and branched GDGT-based proxies for surface sediments from marine, fjord and lake environments in Chile. *Organic Geochemistry*, 89–90, 117–127. doi: 10.1016/j.orggeochem.2015.10.007
- Karner, M. B., DeLong, E. F., & Karl, D. M. (2001). Archaeal dominance in the mesopelagic zone of the Pacific Ocean. *Nature*, 409(6819), 507–510.
- Kawagata, S. (2001). Tasman Front shifts and associated paleoceanographic changes during the last 250,000 years: foraminiferal evidence from the Lord Howe Rise. *Marine Micropaleontology*, 41(3), 167–191. Retrieved from <https://www.sciencedirect.com/science/article/pii/S037783980000058X> doi: [https://doi.org/10.1016/S0377-8398\(00\)00058-X](https://doi.org/10.1016/S0377-8398(00)00058-X)
- Kim, B., & Zhang, Y. G. (2023). Methane Index: Towards a quantitative archaeal lipid biomarker proxy for reconstructing marine sedimentary methane fluxes. *Geochimica et Cosmochimica Acta*. doi: 10.1016/j.gca.2023.06.008
- Kim, J.-H., Schouten, S., Hopmans, E. C., Donner, B., & Sinninghe Damsté, J. S. (2008). Global sediment core-top calibration of the TEX86 paleothermometer in the ocean. *Geochimica et Cosmochimica Acta*, 72(4), 1154–1173. doi: <https://doi.org/10.1016/j.gca.2007.12.010>
- Kim, J.-H., Schouten, S., Rodrigo-Gámiz, M., Rampen, S., Marino, G., Huguet, C., ... Sinninghe Damsté, J. S. (2015). Influence of deep-water derived isoprenoid tetraether lipids on the TEX86H paleothermometer in the Mediterranean Sea. *Geochimica et Cosmochimica Acta*, 150, 125–141. doi: 10.1016/j.gca.2014.11.017
- Kim, J.-H., van der Meer, J., Schouten, S., Helmke, P., Willmott, V., Sangiorgi, F., ... Sinninghe Damsté, J. S. (2010). New indices and calibrations derived from the distribution of crenarchaeal isoprenoid tetraether lipids: Implications for past sea surface temperature reconstructions. *Geochimica et Cosmochimica Acta*, 74(16), 4639–4654. doi: 10.1016/j.gca.2010.05.027
- Kim, J.-H., Villanueva, L., Zell, C., & Sinninghe Damsté, J. S. (2016). Biological source and provenance of deep-water derived isoprenoid tetraether lipids along the Portuguese continental margin. *Geochimica et Cosmochimica Acta*, 172, 177–204. doi: 10.1016/j.gca.2015.09.010
- Kozdon, R., & Kelly, D. C. (2024). Hot Tropical Temperatures During the Paleocene-Eocene Thermal Maximum Revealed by Paired In Situ $\delta^{13}\text{C}$ and

- Mg/Ca Measurements on Individual Planktic Foraminifer Shells. *Paleoceanography and Paleoclimatology*, 39(8), e2023PA004834. doi: 10.1029/2023PA004834
- Kusch, S., Rethemeyer, J., Hopmans, E. C., Wacker, L., & Mollenhauer, G. (2016). Factors influencing ^{14}C concentrations of algal and archaeal lipids and their associated sea surface temperature proxies in the Black Sea. *Geochimica et Cosmochimica Acta*, 188, 35–57. doi: 10.1016/j.gca.2016.05.025
- Kuypers, M. M. M., Blokker, P., Erbacher, J., Kinkel, H., Pancost, R. D., Schouten, S., & Sinninghe Damsté, J. S. (2001). Massive Expansion of Marine Archaea During a Mid-Cretaceous Oceanic Anoxic Event. *Science*, 293(5527), 92–95. Retrieved from <https://science.sciencemag.org/content/sci/293/5527/92.full.pdf> doi: 10.1126/science.1058424
- Lamping, N., Müller, J., Hefter, J., Mollenhauer, G., Haas, C., Shi, X., ... Hillenbrand, C.-D. (2021). Evaluation of lipid biomarkers as proxies for sea ice and ocean temperatures along the Antarctic continental margin. *Climate of the Past*, 17(5), 2305–2326. doi: 10.5194/cp-17-2305-2021
- Lisiecki, L. E., & Raymo, M. E. (2005). A Pliocene-Pleistocene stack of 57 globally distributed benthic $\delta^{18}\text{O}$ records. *Paleoceanography*, 20(1). doi: 10.1029/2004pa001071
- Lo, L., Belt, S. T., Lattaud, J., Friedrich, T., Zeeden, C., Schouten, S., ... Hodell, D. A. (2018). Precession and atmospheric CO₂ modulated variability of sea ice in the central Okhotsk Sea since 130,000 years ago. *Earth and Planetary Science Letters*, 488, 36–45. doi: 10.1016/j.epsl.2018.02.005
- Locarnini, R. A., Mishonov, A. V., Baranova, O. K., Reagan, J. R., Boyer, T. P., Seidov, D., ... others (2024). World ocean atlas 2023, volume 1: Temperature.
- Martens-Habbena, W., Berube, P. M., Urakawa, H., de la Torre, J. R., & Stahl, D. A. (2009). Ammonia oxidation kinetics determine niche separation of nitrifying Archaea and Bacteria. *Nature*, 461(7266), 976–979. Retrieved from <http://dx.doi.org/10.1038/nature08465> doi: doi:10.1038/nature08465
- Martínez, J. (1994). Late Pleistocene palaeocenography of the Tasman Sea: Implications for the dynamics of the warm pool in the western Pacific. *Palaeogeography, Palaeoclimatology, Palaeoecology*, 112(1), 19–62. Retrieved from <https://www.sciencedirect.com/science/article/pii/0031018294901333> doi: https://doi.org/10.1016/0031-0182(94)90133-3
- McKinney, W. (2010). Data structures for statistical computing in Python. In *Proceedings of the 9th Python in science conference* (Vol. 445).
- McManus, J. F., Francois, R., Gherardi, J.-M., Keigwin, L. D., & Brown-Leger, S. (2004). Collapse and rapid resumption of Atlantic meridional circulation linked to deglacial climate changes. *Nature*, 428(6985), 834–837. doi: 10.1038/nature02494
- Pan, A., Yang, Q., Zhou, H., Ji, F., Wang, H., & Pancost, R. D. (2016). A diagnostic GDGT signature for the impact of hydrothermal activity on surface deposits at the Southwest Indian Ridge. *Organic Geochemistry*, 99, 90–101.
- Paulot, F., Jacob, D. J., Johnson, M. T., Bell, T. G., Baker, A. R., Keene, W. C., ... Stock, C. A. (2015). Global oceanic emission of ammonia: Constraints from seawater and atmospheric observations. *Global Biogeochemical Cycles*, 29(8), 1165–1178. Retrieved from <https://doi.org/10.1002/2015GB005106> doi: https://doi.org/10.1002/2015GB005106
- Pedregosa, F., Varoquaux, G., Gramfort, A., Michel, V., Thirion, B., Grisel, O., ... others (2011). Scikit-learn: Machine learning in python. *Journal of Machine Learning Research*, 12, 2825–2830.
- Peng, X., Fuchsman, C. A., Jayakumar, A., Warner, M. J., Devol, A. H., & Ward, B. B. (2016). Revisiting nitrification in the Eastern Tropical South Pacific: A focus on controls. *Journal of Geophysical Research: Oceans*, 121(3), 1667–

1684. doi: 10.1002/2015JC011455

Perruche, C. (2018). Product user manual for the global ocean biogeochemistry hindcast global_reanalysis_bio_001_029. version 1. *Copernicus Marine Environment Monitoring Service*. doi: <http://dx.doi.org/10.25607/OPB-490>

Petit, J. R., Jouzel, J., Raynaud, D., Barkov, N. I., Barnola, J.-M., Basile, I., ... Stievenard, M. (1999). Climate and atmospheric history of the past 420,000 years from the Vostok ice core, Antarctica. *Nature*, 399(6735), 429–436. doi: 10.1038/20859

Polik, C. A., Elling, F. J., & Pearson, A. (2018). Impacts of Paleoecology on the TEX86 Sea Surface Temperature Proxy in the Pliocene-Pleistocene Mediterranean Sea. *Paleoceanography and Paleoclimatology*, 33(12), 1472–1489. doi: 10.1029/2018pa003494

Polovina, J. J., Dunne, J. P., Woodworth, P. A., & Howell, E. A. (2011). Projected expansion of the subtropical biome and contraction of the temperate and equatorial upwelling biomes in the North Pacific under global warming. *ICES Journal of Marine Science*, 68(6), 986–995. doi: 10.1093/icesjms/fsq198

Proctor, C., Coupel, P., Casciotti, K., Tremblay, J.-E., Zakem, E., Arrigo, K. R., & Mills, M. M. (2023). Light, ammonium, pH, and phytoplankton competition as environmental factors controlling nitrification. *Limnology and Oceanography*, 68(7), 1490–1503. doi: 10.1002/lo.12359

Python 3.10. (2010). <https://www.python.org/>. (Python Software Foundation)

Qin, W., Carlson, L. T., Armbrust, E. V., Devol, A. H., Moffett, J. W., Stahl, D. A., & Ingalls, A. E. (2015). Confounding effects of oxygen and temperature on the TEX86 signature of marine Thaumarchaeota. *Proceedings of the National Academy of Sciences of the U.S.A.*, 112(35), 10979–10984.

Rasmussen, S. O., Andersen, K. K., Svensson, A. M., Steffensen, J. P., Vinther, B. M., Clausen, H. B., ... Ruth, U. (2006, mar). A new Greenland ice core chronology for the last glacial termination. *Journal of Geophysical Research: Atmospheres*, 111(D6). Retrieved from <https://doi.org/10.1029/2005JD006079> doi: <https://doi.org/10.1029/2005JD006079>

Rattanasriampaipong, R., Tierney, J., & Abell, J. (2025). *Supplementary Data for ‘A nutrient effect on the TEX₈₆ paleotemperature proxy’*. [Dataset]. Zenodo. doi: 10.5281/zenodo.14806962

Rattanasriampaipong, R., Zhang, Y. G., Pearson, A., Hedlund, B., & Zhang, S. (2022b). *Expanded compilations of isoprenoidal glycerol dialkyl glycerol tetraethers (GDGTs) in supplement to Rattanasriampaipong et al. “Archaeal lipids trace ecology and evolution of marine ammonia-oxidizing archaea”*. [Dataset]. figshare. doi: 10.6084/m9.figshare.20272866.v3

Rattanasriampaipong, R., Zhang, Y. G., Pearson, A., Hedlund, B. P., & Zhang, S. (2022a). Archaeal lipids trace ecology and evolution of marine ammonia-oxidizing archaea. *Proceedings of the National Academy of Sciences*, 119(31), e2123193119. doi: 10.1073/pnas.2123193119

Richey, J. N., & Tierney, J. E. (2016). GDGT and alkenone flux in the northern Gulf of Mexico: Implications for the TEX86 and UK₃₇ paleothermometers. *Paleoceanography*, 31(12), 1547–1561. doi: 10.1002/2016pa003032

Rodrigo-Gámiz, M., Rampen, S. W., de Haas, H., Baas, M., Schouten, S., & Sinninghe Damsté, J. S. (2015). Constraints on the applicability of the organic temperature proxies UK₃₇, TEX₈₆ and LDI in the subpolar region around Iceland. *Biogeosciences*, 12(22), 6573–6590. doi: 10.5194/bg-12-6573-2015

Schouten, S., Forster, A., Panoto, F. E., & Sinninghe Damsté, J. S. (2007). Towards calibration of the TEX86 palaeothermometer for tropical sea surface temperatures in ancient greenhouse worlds. *Organic Geochemistry*, 38(9), 1537–1546. Retrieved from <http://www.sciencedirect.com/science/article/pii/S0146638007001209> doi: <https://doi.org/10.1016/j.orggeochem.2007.05.014>

- 659 Schouten, S., Hopmans, E. C., Schefuss, E., & Sinninghe Damst  , J. S. (2002). Distributional variations in marine crenarchaeotal membrane lipids: a new tool for
660 reconstructing ancient sea water temperatures? *Earth and Planetary Science
661 Letters*, 204(1-2), 265–274.
- 662 Schukies, J. (2018). *Concentrations of glycerol dialkyl glycerol tetraethers (GDGTs)
663 in core top sediments from continental slope off Newfoundland, Orphan Knoll
664 Region*. [Dataset]. PANGAEA. doi: 10.1594/PANGAEA.894305
- 665 Schulte, S., & M  ller, P. J. (2001). Variations of sea surface temperature and
666 primary productivity during Heinrich and Dansgaard-Oeschger events in
667 the northeastern Arabian Sea. *Geo-Marine Letters*, 21(3), 168–175. Retrieved from <https://doi.org/10.1007/s003670100080> doi: 10.1007/
668 s003670100080
- 669 Seierstad, I. K., Abbott, P. M., Bigler, M., Blunier, T., Bourne, A. J., Brook, E., ...
670 Vinther, B. M. (2014). Consistently dated records from the Greenland GRIP,
671 GISP2 and NGRIP ice cores for the past 104 ka reveal regional millennial-scale
672 $\delta^{18}\text{O}$ gradients with possible Heinrich event imprint. *Quaternary Science
673 Reviews*, 106, 29–46. doi: 10.1016/j.quascirev.2014.10.032
- 674 Sikes, E. L., Howard, W. R., Samson, C. R., Mahan, T. S., Robertson, L. G., &
675 Volkman, J. K. (2009). Southern Ocean seasonal temperature and Subtropical
676 Front movement on the South Tasman Rise in the late Quaternary. *Paleo-
677 oceanography*, 24(2). Retrieved from <https://doi.org/10.1029/2008PA001659>
678 doi: <https://doi.org/10.1029/2008PA001659>
- 679 Sinninghe Damst  , J. S., van Bentum, E. C., Reichart, G.-J., Pross, J., & Schouten,
680 S. (2010). A CO₂ decrease-driven cooling and increased latitudinal temper-
681 ature gradient during the mid-Cretaceous Oceanic Anoxic Event 2. *Earth
682 and Planetary Science Letters*, 293(1), 97–103. Retrieved from <https://www.sciencedirect.com/science/article/pii/S0012821X10001299> doi:
683 <https://doi.org/10.1016/j.epsl.2010.02.027>
- 684 Sinninghe Damst  , J. S. (2016). Spatial heterogeneity of sources of branched
685 tetraethers in shelf systems: The geochemistry of tetraethers in the Berau
686 River delta (Kalimantan, Indonesia). *Geochimica et Cosmochimica Acta*, 186,
687 13–31. doi: 10.1016/j.gca.2016.04.033
- 688 Sinninghe Damst  , J. S., Ossebaar, J., Schouten, S., & Verschuren, D. (2012).
689 Distribution of tetraether lipids in the 25-ka sedimentary record of Lake
690 Challa: extracting reliable TEX86 and MBT/CBT palaeotemperatures from
691 an equatorial African lake. *Quaternary Science Reviews*, 50, 43–54. doi:
692 10.1016/j.quascirev.2012.07.001
- 693 Sinninghe Damst  , J. S., Schouten, S., Hopmans, E. C., van Duin, A. C. T.,
694 & Geenevasen, J. A. J. (2002). Crenarchaeol: the characteristic core
695 glycerol dibiphytanyl glycerol tetraether membrane lipid of cosmopolitan
696 pelagic crenarchaeota. *Journal of Lipid Research*, 43(10), 1641–1651. doi:
697 10.1194/jlr.m200148-jlr200
- 698 Sinninghe Damst  , J. S., Warden, L. A., Berg, C., J  rgens, K., & Moros, M. (2022).
699 Evaluation of the distributions of hydroxylated glycerol dibiphytanyl glycerol
700 tetraethers (GDGTs) in Holocene Baltic Sea sediments for reconstruction of
701 sea surface temperature: the effect of changing salinity. *Climate of the Past*,
702 18(10), 2271–2288. doi: 10.5194/cp-18-2271-2022
- 703 Sintes, E., Bergauer, K., De Corte, D., Yokokawa, T., & Herndl, G. J. (2013).
704 Archaeal amoA gene diversity points to distinct biogeography of ammonia-
705 oxidizing Crenarchaeota in the ocean. *Environmental Microbiology*, 15, 1647–
706 1658.
- 707 Sloyan, B. M., & O’Kane, T. J. (2015). Drivers of decadal variability in the Tasman
708 Sea. *Journal of Geophysical Research: Oceans*, 120(5), 3193–3210. Retrieved
709 from <https://doi.org/10.1002/2014JC010550> doi: <https://doi.org/10.1002/2014JC010550>

- 714 Smith, J. M., Casciotti, K. L., Chavez, F. P., & Francis, C. A. (2014, aug). Differential contributions of archaeal ammonia oxidizer ecotypes to nitrification in
 715 coastal surface waters. *The ISME Journal*, 8(8), 1704–1714. Retrieved from
 716 <https://doi.org/10.1038/ismej.2014.11> doi: 10.1038/ismej.2014.11
- 717 Sonzogni, C., Bard, E., & Rostek, F. (1998). TROPICAL SEA-SURFACE
 718 TEMPERATURES DURING THE LAST GLACIAL PERIOD: A VIEW
 719 BASED ON ALKENONES IN INDIAN OCEAN SEDIMENTS. *Qua-*
 720 *tertary Science Reviews*, 17(12), 1185–1201. Retrieved from <https://www.sciencedirect.com/science/article/pii/S0277379197000991> doi:
 721 [https://doi.org/10.1016/S0277-3791\(97\)00099-1](https://doi.org/10.1016/S0277-3791(97)00099-1)
- 722 Suthhof, A., Ittekkot, V., & Gaye-Haake, B. (2001). Millennial-scale oscillation
 723 of denitrification intensity in the Arabian Sea during the Late Quaternary
 724 and its potential influence on atmospheric N₂O and global climate. *Global*
 725 *Biogeochemical Cycles*, 15(3), 637–649. doi: 10.1029/2000GB001337
- 726 Talley, L. D., Pickard, G. L., Emery, W. J., & Swift, J. H. (2011). *Descriptive phys-*
 727 *ical oceanography: an introduction* (6th ed.). Academic press. doi: <https://doi.org/10.1016/C2009-0-24322-4>
- 728 Tang, W., Ward, B. B., Beman, M., Bristow, L., Clark, D., Fawcett, S., ... Zhang,
 729 Y. (2023). Database of nitrification and nitrifiers in the global ocean. *Earth*
 730 *System Science Data*, 15(11), 5039–5077. doi: 10.5194/essd-15-5039-2023
- 731 Taylor, K. W. R., Huber, M., Hollis, C. J., Hernandez-Sanchez, M. T., & Pancost,
 732 R. D. (2013). Re-evaluating modern and Palaeogene GDGT distributions:
 733 Implications for SST reconstructions. *Global and Planetary Change*, 108,
 734 158–174. doi: 10.1016/j.gloplacha.2013.06.011
- 735 Tesdal, J.-E., Galbraith, E. D., & Kienast, M. (2013). Nitrogen isotopes in bulk ma-
 736 rine sediment: linking seafloor observations with subseafloor records. *Biogeosciences*,
 737 10(1), 101–118. doi: 10.5194/bg-10-101-2013
- 738 Tierney, J. E., Pausata, F. S. R., & DeMenocal, P. (2016). Deglacial Indian monsoon
 739 failure and North Atlantic stadials linked by Indian Ocean surface cooling. *Nature*
 740 *Geoscience*, 9(1), 46–50. doi: 10.1038/ngeo2603
- 741 Tierney, J. E., Poulsen, C. J., Montañez, I. P., Bhattacharya, T., Feng, R., Ford,
 742 H. L., ... Zhang, Y. G. (2020). Past climates inform our future. *Science*,
 743 370(6517), eaay3701. doi: 10.1126/science.aay3701
- 744 Tierney, J. E., & Tingley, M. P. (2014). A Bayesian, spatially-varying calibration
 745 model for the TEX86 proxy. *Geochimica et Cosmochimica Acta*, 127, 83–106.
 746 doi: 10.1016/j.gca.2013.11.026
- 747 Tierney, J. E., & Tingley, M. P. (2015a). NOAA/WDS Paleoclimatology - Global
 748 TEX86 Surface Sediment Database. [Dataset]. NOAA National Centers for En-
 749 vironmental Information. doi: <https://doi.org/10.25921/wt2r-sc81>
- 750 Tierney, J. E., & Tingley, M. P. (2015b). A TEX 86 surface sediment database and
 751 extended Bayesian calibration. *Scientific Data*, 2(1), 1–10.
- 752 Tierney, J. E., & Tingley, M. P. (2018). BAYSPLINE: A New Calibration for the
 753 Alkenone Paleothermometer. *Paleoceanography and Paleoclimatology*, 33(3),
 754 281–301. doi: 10.1002/2017PA003201
- 755 Tierney, J. E., Ummenhofer, C. C., & DeMenocal, P. B. (2015). Past and future
 756 rainfall in the Horn of Africa. *Science Advances*, 1(9), e1500682. doi: 10.1126/
 757 sciadv.1500682
- 758 Tilburg, C. E., Subrahmanyam, B., & O'Brien, J. J. (2002, may). Ocean color vari-
 759 ability in the Tasman Sea. *Geophysical Research Letters*, 29(10), 124–125. Re-
 760 trieval from <https://doi.org/10.1029/2001GL014071> doi: <https://doi.org/10.1029/2001GL014071>
- 761 Trommer, G., Siccha, M., van der Meer, M. T. J., Schouten, S., Sinninghe Damsté,
 762 J. S., Schulz, H., ... Kucera, M. (2009). Distribution of Crenarchaeota
 763 tetraether membrane lipids in surface sediments from the Red Sea. *Organic*
 764 *Geochemistry*, 40(6), 724–731. doi: 10.1016/j.orggeochem.2009.03.001

- 769 Tyrrell, T. (1999). The relative influences of nitrogen and phosphorus on oceanic
 770 primary production. *Nature*, *400*(6744), 525–531. Retrieved from <https://doi.org/10.1038/22941> doi: 10.1038/22941
- 772 Uda, I., Sugai, A., Itoh, Y. H., & Itoh, T. (2001). Variation in molecular species of
 773 polar lipids from *Thermoplasma acidophilum* depends on growth temperature.
 774 *Lipids*, *36*(1), 103–105.
- 775 van der Weijst, C. M. H., van der Laan, K. J., Peterse, F., Reichart, G.-J., San-
 776 giorgi, F., Schouten, S., ... Sluijs, A. (2022). A 15-million-year surface- and
 777 subsurface-integrated TEX86 temperature record from the eastern equatorial
 778 Atlantic. *Clim. Past*, *18*(8), 1947–1962. doi: 10.5194/cp-18-1947-2022
- 779 van Helmond, N. A. G. M., Sluijs, A., Reichart, G.-J., Sinninghe Damsté, J. S.,
 780 Slomp, C. P., & Brinkhuis, H. (2014). A perturbed hydrological cycle
 781 during Oceanic Anoxic Event 2. *Geology*, *42*(2), 123–126. Retrieved from
 782 <https://doi.org/10.1130/G34929.1> doi: 10.1130/g34929.1
- 783 Varma, D., Hopmans, E. C., van Kemenda, Z. R., Kusch, S., Berg, S., Bale, N. J.,
 784 ... Schouten, S. (2024). Evaluating isoprenoidal hydroxylated GDGT-based
 785 temperature proxies in surface sediments from the global ocean. *Geochimica et*
Cosmochimica Acta, *370*, 113–127. doi: 10.1016/j.gca.2023.12.019
- 787 Varma, D., Hopmans, E. C., van Kemenda, Z. R., Kusch, S., Berg, S., Bale, N. J.,
 788 ... Schouten, S. (2024). *OHGDGT global surface sediment data*. [Dataset].
 789 PANGAEA. doi: 10.1594/PANGAEA.964885
- 790 Villanueva, L., Schouten, S., & Sinninghe Damsté, J. S. (2015). Depth-related
 791 distribution of a key gene of the tetraether lipid biosynthetic pathway in ma-
 792 rine Thaumarchaeota. *Environmental Microbiology*, *17*, 3527–3539. doi:
 793 10.1111/1462-2920.12508
- 794 Virtanen, P., Gommers, R., Oliphant, T. E., Haberland, M., Reddy, T., Courn-
 795 peau, D., ... others (2020). Scipy 1.0: Fundamental algorithms for scientific
 796 computing in python. *Nature Methods*, *17*(3), 261–272.
- 797 Ward, B. B. (2008). Chapter 5 - Nitrification in Marine Systems. In D. G. Capone,
 798 D. A. Bronk, M. R. Mulholland, & E. J. B. T. N. i. t. M. E. S. E. Car-
 799 penter (Eds.), (pp. 199–261). San Diego: Academic Press. doi: 10.1016/
 800 B978-0-12-372522-6.00005-0
- 801 Ward, B. B. (2011). Nitrification in the Ocean. In *Nitrification* (pp. 323–345). doi:
 802 10.1128/9781555817145.ch13
- 803 Wei, B., Jia, G., Hefter, J., Kang, M., Park, E., Wang, S., & Mollenhauer, G.
 804 (2020). Comparison of the UK₃₇, LDI, TEX₈₆^H, and RI-OH temperature proxies
 805 in sediments from the northern shelf of the South China Sea. *Biogeosciences*,
 806 *17*(17), 4489–4508. doi: 10.5194/bg-17-4489-2020
- 807 Weijers, J. W. H., Schouten, S., Spaargaren, O. C., & Sinninghe Damsté, J. S.
 808 (2006). Occurrence and distribution of tetraether membrane lipids in soils:
 809 Implications for the use of the TEX86 proxy and the BIT index. *Organic*
 810 *Geochemistry*, *37*(12), 1680–1693. doi: 10.1016/j.orggeochem.2006.07.018
- 811 Wuchter, C., Abbas, B., Coolen, M. J. L., Herfort, L., van Bleijswijk, J., Timmers,
 812 P., ... Sinninghe Damsté, J. S. (2006). Archaeal nitrification in the ocean.
 813 *Proceedings of the National Academy of Sciences of the U.S.A.*, *103*, 12317–
 814 12322.
- 815 Wuchter, C., Schouten, S., Coolen, M. J. L., & Sinninghe Damsté, J. S. (2004).
 816 Temperature-dependent variation in the distribution of tetraether membrane
 817 lipids of marine Crenarchaeota: Implications for TEX86 paleothermometry.
 818 *Paleoceanography*, *19*(4). doi: 10.1029/2004PA001041
- 819 Yang, H., Lohmann, G., Krebs-Kanzow, U., Ionita, M., Shi, X., Sidorenko, D., ...
 820 Gowan, E. J. (2020). Poleward Shift of the Major Ocean Gyres Detected in a
 821 Warming Climate. *Geophysical Research Letters*, *47*(5), e2019GL085868. doi:
 822 10.1029/2019GL085868

- 823 Yang, Y., Gao, C., Dang, X., Ruan, X., Lü, X., Xie, S., ... Yang, H. (2018).
824 Assessing hydroxylated isoprenoid GDGTs as a paleothermometer for the
825 tropical South China Sea. *Organic Geochemistry*, 115, 156–165. doi:
826 10.1016/j.orggeochem.2017.10.014
- 827 Yool, A., Martin, A. P., Fernández, C., & Clark, D. R. (2007). The significance of
828 nitrification for oceanic new production. *Nature*, 447(7147), 999–1002. doi: 10
829 .1038/nature05885
- 830 Zachos, J., Dickens, G. R., & Zeebe, R. E. (2008). An early Cenozoic perspective on
831 greenhouse warming and carbon-cycle dynamics. *Nature*, 451, 279. Retrieved
832 from <https://doi.org/10.1038/nature06588> doi: 10.1038/nature06588
- 833 Zachos, J., Pagani, M., Sloan, L., Thomas, E., & Billups, K. (2001, apr). Trends,
834 Rhythms, and Aberrations in Global Climate 65 Ma to Present. *Science*,
835 292(5517), 686–693. Retrieved from <https://doi.org/10.1126/science.1059412> doi: 10.1126/science.1059412
- 836 Zhang, Y. G., Zhang, C. L., Liu, X.-L., Li, L., Hinrichs, K.-U., & Noakes, J. E.
837 (2011). Methane Index: a tetraether archaeal lipid biomarker indicator for
838 detecting the instability of marine gas hydrates. *Earth and Planetary Science
Letters*, 307(3-4), 525–534.
- 839
- 840